# Impact of multi-component description of hydrophilic fuel droplets in propagating spray flames

Fernando Luiz Sacomano Filho[a,*], Luís Eduardo de Albuquerque Paixão e Freire de Carvalho[a], Artur Carvalho Santos[b], Aymeric Vié[b,c], Jeroen Adrianus van Oijen[d]

[a]*Laboratory of Environmental and Thermal Engineering, Universidade de São Paulo, São Paulo, Brazil.*
[b]*Laboratoire EM2C, CNRS, CentraleSupelec, Université Paris-Saclay, Gif-sur-Yvette, France.*
[c]*Fédération de Mathématiques, CentraleSupelec, Université Paris-Saclay, Gif-sur-Yvette, France.*
[d]*Department of Mechanical Engineering, Technische Universiteit Eindhoven, Eindhoven, The Netherlands.*

**Abstract**

The need for an accurate description of the fuel composition is emerging in recently published studies on the interaction of droplets and flames. In this context, hydrophilic fuels are of particular importance, since they are expected to interact with the water formed during combustion reactions. The impact of such interactions onto the reaction process is still not explored enough. This work aims to contribute to the understanding of such interactions by investigating the impact of accurately describing the heat and mass transfers on hydrophilic fuel droplets interacting with flames. For that, a recently proposed phase change model is employed, demonstrated to be one of the few capable of characterizing the differential diffusion of vapor into the gas phase for hydrophilic fuels interacting with reacting flows. Numerical simulations of freely propagating flames in quiescent droplet mists are conducted with a detailed chemistry description. Different scenarios focus on the impact of water addition in the gaseous or liquid phase. Results demonstrated the multi-component phase change significantly impacts the flame speed in humid air and/or with hydrous ethanol, and neglecting this effect leads to strong miscalculation in flame speed. This is shown to be a consequence of the hydrophilic property of the chosen fuel, which allows the conversion from single-component to multi-component droplets, thus modifying the flame structure.

*Keywords:* Multi-component droplets, Spray combustion, Phase change modeling, Differential diffusion, Ethanol

## Novelty and significance statement

- Differential diffusion is rigorously accounted for with a new phase change model in flames propagating in droplet mists of a hydrophilic fuel, i.e., ethanol.
- The multi-component modeling is necessary even when considering the injection of pure hydrophilic fuel.

*Corresponding author
*Email address:* fernando.sacomano@usp.br (Fernando Luiz Sacomano Filho)

- When the multi-component description of the liquid fuel is enabled, flame speeds become higher than those values achieved with the single-component approach.
- Air humidity interacts with hydrophilic fuel droplets delivering higher flame speed values.
- A novel justification is presented for the observed higher flame speed values of flames propagating in droplet mists when compared to single-phase flames.

**Author contributions statement**

F.L.S.F.: designed and performed research, analyzed and post-processed data, and wrote and revised the paper. L.E.A.P.F.C.: performed simulations, analyzed and post-processed data, and revised the paper. A.C.S.: supported the model implementations, analyzed data, and revised the paper. A.V.: provided algorithms, analyzed data, and revised the paper. J.A.v.O.: provided software, analyzed data, and revised the paper.

## 1. Introduction

Typical commercial fuels are composed of a large number of species and require multi-component modeling for the numerical description of spray flames [1–4]. Investigations about the multi-component description of droplets in non-reacting atmospheres are found in the literature for single droplets (e.g. [3–11]) and spray flows (e.g. [12]). However, the interaction of multi-component droplets with reacting flows is not extensively explored. Spray combustion simulations are commonly conducted with single-component surrogate fuels (e.g. [13, 14]) to avoid the complexity of modeling multi-component chemical kinetics and droplet phase change.

From the published works accounting for multi-component droplets in reacting flows (e.g. [1, 2, 15–21]), both [1, 2] stand out. Shastry et al. [1] investigated one-dimensional flames propagating in multi-component sprays using a detailed description of the chemistry. Alkane mixtures representing Jet-A surrogates were evaluated following the ideal vapor-liquid equilibrium (VLE) approach and without considering differential vapor diffusion into the gas flow. The importance of the multi-component description of droplets is noticed in terms of the stratified mass exchange caused by the different vapor pressures of different components. Differential diffusion effects are able to be modeled in the approach employed in [2], which also investigated alkane mixtures representing Jet-A surrogates. 1D Counterflow spray flames were simulated using a detailed description of the chemistry. Results outline that differential diffusion effects are necessary for modeling multi-component spray combustion.

All these previous studies considered mixtures of long hydrocarbons. When considering alcohols, the number of species is usually small in a commercial fuel (e.g., ethanol). However, these hydrophilic substances can absorb the air humidity and the water formed during combustion [3, 22, 23] and, consequently, interact with the reacting flow. Such an interaction is poorly understood, as this topic has not been sufficiently explored in the literature. The fuel hydrophilicity reinforces the importance of the multi-component description of droplets for both reacting and non-reacting atmospheres. Nevertheless, care must be taken on describing the heat and mass transfer of hydrophilic droplets. As demonstrated in [3], there are limitations in different models available in the literature to accurately describe droplets' heat and mass transfer processes in

reacting atmospheres. Recently new models were proposed [3, 4, 24], which can accurately describe the differential diffusion of vapor into the carrier phase for hydrophilic and non-hydrophilic droplets interacting with general reacting flows. In view of the correct description of the gas phase dynamics, which may enable or disable the simultaneous occurrence of condensation and evaporation mechanisms for individual species, the model proposed in [3] is employed in the present work.

Within the context of one-dimensional simulations conducted with a detailed description of the chemistry, flames propagating in droplet mists have been demonstrated as an important setup to fill an old gap in the research of spray combustion. As well observed by Versaevel [25], spray combustion test cases are mainly found in two extreme setups: single-droplet or polydisperse flows. The last case predominantly involves turbulent carrier phase flows and is not far from real application flames, which implies complex flow configurations. Since that study, new experimental and numerical setups have been proposed (e.g., [6, 26–31]) to reduce the gap between these two extreme setups. Recently, contributions following the numerical setup of one-dimensional flames propagating in droplet mists coupled with a detailed description of the chemistry have been increasing in the literature, e.g., [1, 25, 32–36]. Although the geometrical simplifications are clear in such a numerical setup, it allows a good adherence with experimental measurements as shown in [25]. Furthermore, such a setup is quite effective for evaluating parametric variations in ambient conditions (e.g., temperature and pressure) and in the characteristics of the two-phase flow (e.g., initial droplet diameter, gas and liquid composition).

With the objective to contribute to the understanding of the interactions of hydrophilic fuel droplets with reacting flows, this work presents numerical simulations of laminar flames propagating in quiescent droplet mists. In contrast to previous studies, a rigorous modeling approach [3] for the heat and mass transfer on droplets is considered, which can accurately describe the energy and the mass transport of both hydrophilic and non-hydrophilic fuels in reacting and non-reacting flows. According to the adopted framework, the investigations conducted here complement and give sequence to the previous studies presented by Shastry et al. [1] and Bonanni and Ihme [2], which also present investigations of spray flames in one-dimensional domains including a detailed description of the chemistry and multi-component droplet heat and mass transfer models. Here, due to the emphasis placed on the hydrophilic behavior, effects of different liquid composition and the consideration of air humidity are systematically analyzed for different equivalence ratios.

The paper is structured as follows. After this introduction, modeling approaches are concisely described. Results are presented first, focusing on the impact of air humidity and then on the water content in the fuel. A specific study about the faster flames observed for two-phase flows compared to single-phase ones is presented. The paper ends with conclusions.

## 2. Modeling approaches

The one-dimensional reacting flow solver CHEM1D [37] was used for the numerical simulations. It has been extended with a Lagrangian spray solver to study flames propagating in fuel and non-fuel droplet mists [33, 34, 36]. Simulations of unstrained laminar flames propagating in quiescent mono-dispersed isotropic sprays are presented in this manuscript. Similar to what was done in [1, 25, 32–36], the following assumptions are used: (a) the multi-dimensional characteristic of

the droplets dispersion is not considered; and (b) mists are diluted, thereby no interaction between droplets is accounted for. In the following, the resolved equations are briefly presented.

### *2.1. Gas Phase*

The description of the carrier phase follows a variable-density low Mach number formulation. Following the strategies presented in [33, 36–39], the set of equations employed here is:

$$\frac{d\dot{m}}{dx} = \sum_k S_k, \tag{1}$$

$$\frac{d(\dot{m}Y_i)}{dx} - \frac{d}{dx}\left(\rho Y_i V_i\right) = \dot{\omega}_i + \delta_{ik} S_k, \tag{2}$$

$$\frac{d(\dot{m}h)}{dx} = -\frac{d}{dx}\left[-\lambda\frac{dT}{dx} + \rho\sum_{i=1}^{N} Y_i h_i V_i - RT\sum_{i=1}^{N}\frac{D_i^T}{X_i M_i}\frac{dX_i}{dx}\right] + S_{\mathrm{h}}, \tag{3}$$

where $\dot{m} = \rho u$ is the mixture mass flux, $x$ is the spatial coordinate, and $S_k$ is the source term of vapor species $k$. $Y_i$ is the mass fraction of the species $i \in [1, N_s - 1]$, $N_s$ is the total number of species, $V_i$ is the diffusion velocity, $\dot{\omega}_i$ is the reaction rate, and $\delta_{ik}$ is the Kronecker delta. $h$ is the absolute enthalpy of the mixture, $h_i$ is the absolute enthalpy of each transported species i, while $S_{\mathrm{h}}$ denotes the coupling term between phases. The first term on the RHS of Eq. 3 refers to the heat flux, in which $\lambda$ is the thermal conductivity, $T$ is the temperature, $R$ is the gas constant, $D_i^T$ is the thermal diffusion coefficient, $X$ is the molar fraction, and $M$ is the molar mass. The computation of the diffusion coefficients ($D_{i,m}$ and $D_i^T$) is performed following Ern and Giovangigli [40].

Although more recent chemical mechanisms are available in the literature to describe the oxidation of ethanol in air [41], the mechanism proposed by Marinov [42] was ultimately chosen to conduct the presented analysis. It describes ethanol oxidation in air by means of 57 species and 379 intermediate reactions. Marinov's mechanism was found to be more robust and allowed more stable solutions for the more than 4,000 simulations used for the present study [1]. Preliminary analyses with other mechanisms showed that, although absolute values of flame speed and specific quantities may change slightly when considering different mechanisms, no changes were noticed for the trends and conclusions discussed hereafter. In other words, as is the nature of extensive parametric studies, a stable, cost-efficient, and sufficient reaction mechanism such as Marinov's is employed in order to allow the analysis of an extensive set of conditions without penalty to the takeaways presented herein.

[1] It is essential to mention that, in principle, the maximum number of species and reactions that can be used in CHEM1D is only limited by computational resources (memory). Typically, mechanisms of about a few hundred species and a few thousand reactions can be used on a modern desktop computer. Accordingly, the software does not impose a restriction for the usage of other mechanisms.

*2.2. Liquid Phase*

Since multi-component droplets are accounted for, the main changes in the liquid phase modeling compared to the previous works [33, 34, 36] refer to the heat and mass transfer. Herein, the model of [3] is applied, which accounts for the differential diffusion of vapor into the gas phase [2]

Heat and mass transfer on a droplet are given by:

$$\dot{q}_d = 4\pi R\lambda \frac{Nu}{2}(T_\infty - T_s) + \sum_k \dot{m}_{d,k} L_k, \qquad \dot{m}_d = -4\pi R_d \rho D_k \frac{Sh_k}{2} B_{M,k}. \tag{4}$$

where $\dot{q}_d$ is the heat transfer rate, $R_d$ the droplet radius, $\lambda$ the heat conductivity of the gaseous mixture, $Nu$ the Nusselt number, $\dot{m}_d$ the mass transfer rate, $\dot{m}_{d,k}$ the mass transfer rate of vapor species $k$, $L_k$ the vaporization enthalpy of species $k$, $\rho$ the mixture density, $D_k$ the multi-component diffusion coefficient, and $Sh_k$ the Sherwood number of vapor species $k$. Subscript $s$ refers to quantities evaluated at the droplet surface. By adopting uniform temperature and composition in the droplet interior $\dot{q}_d = m_d\left(\sum_k Y_{L,k} c_{L,k}\right) dT_d/dt$, where $Y_{L,k}$ is the liquid mass fraction and $c_{L,k}$ is the liquid specific heat of vapor species $k$. Following [5], a general approach is to consider that:

$$Nu = \frac{\ln|B_T + 1|}{B_T} Nu^0, \qquad Sh_k = \frac{\ln\left|B_{M,k} + 1\right|}{B_{M,k}} Sh_k^0, \tag{5}$$

$$Nu^0 = 2 + 0.57 Re^{1/2} Pr^{1/3}, \qquad Sh_k^0 = 2 + 0.57 Re^{1/2} {Sc_k}^{1/3}, \tag{6}$$

where $Nu^0$ refers to empirical correlations derived from non-evaporating moving droplets, and $Sh_k^0$ is its analogous for mass transfer (see Eq. 6). $Re = \rho|u_\infty - u_d|d/\mu$ is the Reynolds number, $u_\infty$ the bulk flow velocity, $u_d$ and $d$ the droplet velocity and diameter, $\mu$ the dynamic viscosity, $Pr$ the Prandtl number, and $Sc_k = \mu/\rho D_k$ the species $k$ Schmidt number. $B_T$ and $B_{M,k}$ are the Spalding numbers for energy and species $k$:

$$B_T = \frac{(T_\infty - T_s)\sum_k c_{p,k}\dot{m}_{d,k}}{\dot{q}_d - \sum_k \dot{m}_{d,k} L_k}, \qquad B_{M,k} = \frac{\dot{m}_d Y_{k,s} - \dot{m}_d Y_{k,\infty}}{\dot{m}_{d,k} - \dot{m}_d Y_{k,s}}. \tag{7}$$

The multi-component diffusion coefficient $D_k$ is computed with the Wilke's approach [44], as in [3, 4]. Binary diffusion coefficients are computed with the Fuller-Giddings method [45]. Predominantly, the analysis conducted with the multi-component (MC) approach considers a non-ideal VLE approach by using the van Laar model [46], which is in agreement with the characteristics of ethanol and water mixtures (see, e.g., [3]). However, simulations are also conducted with Raoult's law [46] for VLE modeling in order to give support to important discussions. The surrounding gas properties used for droplet phase change (i.e., $\mu$, $\lambda$, $c_p$, and $D_{ij}$) are computed following [34], where the gas composition in the far field follows the species diluted approach (SD) including all participating species. The procedure adopted to couple both phases is detailed in [33], which has been straightforwardly extended to multi-component mists.

[2] In [4], it has been shown that this model degenerates to the one of Abramzon and Sirignano [43], when the number of species reduce to one. In this way, a single approach is sufficient to conduct simulations for single- and multi-component scenarios.

Bearing in mind the objective of the present work to contribute to the understanding of the interaction of hydrophilic fuel sprays with flames, the integral (0D) description of the droplets heat and mass transfer is elected in tandem with other typical assumptions for CFD solvers (e.g., spherical droplets, point-particle, Fick's law) such that the proposed conclusions are in agreement with these applications. Hence, the presented analysis assumes that the liquid properties vary with time but are uniform inside a droplet, i.e., infinite liquid conductivity and diffusivity (ILCD) are adopted. Although the model proposed in [3] has no restriction about the inclusion of the internal discretization of droplets, the ILCD simplification is assumed since the evaporation and condensation of individual species are triggered by the gas phase modeling, which does not depend on the description of the droplet interior. Therefore, the ILCD assumption is sufficient as a first approach to evaluate the importance of the multi-component modeling even if the discretization of the droplet's interior is neglected. Following this choice, we are able to conduct isolate analyses and avoid the combined effects of vapor transport through the gas film with the discretization of its interior, which may mask the contribution of each modeling part. According to this assumption, the obtained results can be seen as a reference for further and more complex studies accounting for a more detailed description of the droplet interior. Furthermore, these results complement and sequence the previous studies presented in [1] and [2], which consider the same modeling strategy.

### *2.3. Flame speed calculation*

Great part of the conducted discussion in section 4 is based on the laminar flame speed, a major quantity for turbulent flame modeling. Therefore, it is important to know how this quantity is computed in CHEM1D. The procedure follows the flamelet theory described in [47]. First, the flame speed $v_f$ is defined based on the propagation velocity of the corresponding density iso-contour:

$$v_f = \left[\frac{1}{\sigma}\frac{d(\sigma\rho u)}{dx} + \rho K\right] \Big/ \left(\frac{d\rho}{dx}\right), \tag{8}$$

where $K$ is the scalar stretch and $\sigma$ is a measure for the flame area on the flame surfaces through which transport takes place. The gas velocity $u_g$ and the burning velocity $s_L$ are determined at the position of the inner layer, which is chosen as the location of the maximum heat release rate. The burning velocity follows the difference between flame speed and gas velocity: $s_L = v_f - u_g$.

In specific for steady flames, as considered in the present study, $v_f = 0$ and, therefore, $s_L = -u_g$. Note that this burning velocity changes in the flame because of the density variation. Therefore, it is useful to consider the mass burning rate $\dot{m}_b = \rho s_L$. Finally, the laminar burning velocity with respect to the unburnt side: $s_{L,u} = \dot{m}_b/\rho_u$, is then achieved. The $s_{L,u}$ is the quantity employed in the presented analysis hereafter.

## 3. Numerical setup

To investigate the interactions of hydrophilic fuel droplets with reacting flows, droplets are injected 30 mm upstream of the flame front with an initial diameter ($d_0$) of 50 $\mu$m. Variations of initial droplet diameter have been investigated previously in [33, 34, 36] for single-component fuel and non-fuel droplets. Herein, the initial droplet size has been selected as an intermediate value between small droplets $< 25$ $\mu$m, which predominantly interact with the flame pre-heating

zone, and large ones > 75 $\mu$m, which respectively tend to penetrate far into the flame oxidation zone. The one-dimensional computational domain extends from -100 mm to 400 mm, in which the flame front is held at the coordinate 0.0 mm[3]. For the different tested scenarios, variations of the overall equivalence ratio ($\phi_{over}$), i.e. the $\phi$ equivalent to when the spray is completely pre-vaporized, are considered. By setting an overall equivalence ratio $\phi_{over}$, the mass flow of liquid is adjusted accordingly [33]. In all simulated cases, the inlet and initial droplet temperatures are 298 K [4]. Here, humid air refers to 100% relative humidity, i.e. $X_{H_2O} = 0.032$ at 298 K.

In order to achieve the presented results, the procedure to obtain converged solutions is as follows. A start case is first obtained from gaseous flame simulations for a given scenario. For that, a stoichiometric flame is considered and the amount of liquid is gradually increased up to obtain 100% of fuel being injected as a liquid at the desired injection position. As a start case is achieved, variations in $\phi_{over}$ are step-wise computed until the lean and rich quenching limits are reached. The CPU time for a simulation strongly depends on the number of chosen control volumes, the applied modeling approaches, and the actual value of $\phi_{over}$. For instance, a step in $\phi_{over}$ near the stoichiometry may take a few minutes, while the same step but close to the rich quenching limit may take several hours or even days, if they converge at all. The strong variability of a single one-dimensional flame's run time corroborates the choice of a stable, cost-efficient and sufficient reaction mechanism such as Marinov's. For the present computations, the number of control volumes varied from 500 to 1000. For the majority of the simulated flames, a converged solution could be obtained for less than 300 points as an adaptive grid method [37] is applied. However, a high number of cells were used to facilitate some post-processing routines. Simulations were run until convergence was reached, which follows the same criteria originally applied for gas flames in [37]. Details about numerical procedures applied for the numerical coupling of Eulerian and Lagrangian routines can be found in [33, 34, 48]. In contrast to the methods described in [48], herein the ordinary differential equations used to describe the Lagrangian phase are solved using the fixed-order Runge-Kutta algorithm of 5$^{th}$ order proposed in [49].

## 4. Results

Results are presented in three sections. The focus is on the laminar flame speed and the influence of the multi-component modeling on this quantity. The first section concentrates on the impacts of the multi-component modeling on flames propagating in droplets mists of pure hydrophilic fuel in humid and dry air. The second investigates the consequences of considering droplets composed of a mixture of such a fuel and water for flames propagating in sprays. A specific discussion about the faster flames observed for two-phase flows compared to single-phase (SP) ones is conducted in the third section, where a novel justification for this phenomenon is presented.

[3]The flame front position is where the gas temperature is increased by 200 K compared to the inlet temperature.

[4]It must be remembered that the mixture's absolute enthalpy differs between SP and spray cases. The evaporative cooling induced by the spray has been shown to decrease the flame speed in [33] and this trend must be considered in the comparison between gaseous and spray cases.

### 4.1. *Pure hydrophilic fuel droplet in dry and humid air*

The laminar flame speeds of spray flames in humid and dry air are presented in Fig. 1. Single-phase laminar flame speeds are also included for reference in both conditions, i.e. humid and dry air. The general trends are found to be consistent with the literature (e.g. [25, 32, 34, 36]). Here, the focus is on the distinct behaviors observed when different modeling assumptions and atmospheric conditions are considered.

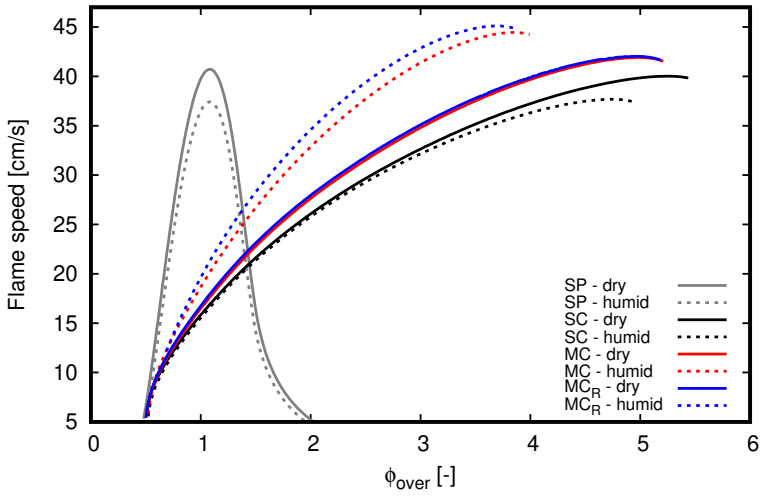


Figure 1: Laminar flame speed by overall equivalence ratio of single phase (SP) and two-phase freely propagating flames for humid and dry air. In all mists, pure ethanol is injected. SC denotes single component and MC multi-component droplet model. The label $MC_R$ specifically refers to the MC model computed with the ideal VLE approach, i.e., Raoult's law.

Focusing first on the results achieved with the single component (SC) approach, as it occurs for single-phase flames, the inclusion of water vapor into the air stream leads to lower flame speed values when compared to the results achieved with dry air. The consideration of this reaction product already in the reactants stream may justify the anticipation of the quenching point to lower values of $\phi_{over}$, when compared with the dry air cases. However, the characteristic in which both SC cases deviate between each other is to be highlighted. The deviations between both cases increase as $\phi_{over}$ counter-intuitively increases, as less vapor is proportionally found in rich mixtures than in lean ones. Nevertheless, this characteristic resembles what is observed for the fastest SP flames. According to Liang et al. [50], the chemical kinetic effects of water addition over the single-phase laminar flame speed are very small compared to thermophysical effects. In that study, the physical and chemical effects of water addition in ethanol over laminar flame speeds were isolated through a pseudo-species approach, and the chemical kinetic effects were very small. Hence, Liang et al. [50] attributed the influence of water addition over ethanol flame speeds to be of a physical nature.

The importance of the consideration of a multi-component approach to describe hydrophilic fuel droplets is evident in Fig. 1, regardless of the VLE approach. Since it is well known that ethanol and water mixtures follow a non-ideal VLE, discussions presented hereafter refer to the non-ideal VLE approach unless explicitly mentioned otherwise. By comparing SC and MC cases

in dry air, flame speeds with the MC approach are always higher and deviations increase to a maximum of approximately 10% as $\phi_{\text{over}}$ increases. By considering the MC approach, the water formed in the combustion process is allowed to interact with the hydrophilic droplets[5]. Regardless of the VLE approach, droplet temperatures are bounded by the boiling point temperatures of individual components, i.e., $T_{b,C_2H_5OH} = 351.5\ K$ and $T_{b,H_2O} = 373.2\ K$. Hence, when droplets do not evaporate before reaching the reaction zone, a cold liquid structure interacts with the flame. When the MC approach is turned on, water formed in the combustion process is able to condensate on the droplet surface, releasing heat to heat up both gaseous and liquid phases. Specifically, condensation causes the opposite effect of evaporative cooling.

Water condensation on droplets surfaces was predicted before starting this study, but such an impact on flame speeds was unexpected. The presented results are novel, but not as contrasting as those seen in Fig. 1 for the MC approach in humid atmospheres. As observed for SP cases and for those of two-phase flows using the SC approach, by adding humidity, the laminar flame speed decreases for the entire $\phi_{\text{over}}$ span. In contrast, with the inclusion of humidity when modeling droplets with an MC approach, the flame propagation becomes faster as $\phi_{\text{over}}$ increases. Flames are about 20% faster than those computed in dry air. In humid air, the differences are even larger between MC and SC, but what is more contrasting is the different behaviors when adding humidity: while humid air leads to slightly decreased flame speeds in the SC approach, there is a very strong increase in flame speed in the MC approach.

To investigate these behaviors, ethanol, and water mass fractions profiles of the gaseous mixture are presented in Fig. 2 with the gas temperature of flames for $\phi_{\text{over}} = 3.0$. The overall equivalence ratio $\phi_{\text{over}} = 3.0$ is chosen since deviations among scenarios are more pronounced for rich mixtures. However, as seen on the next colormaps, these are not exclusive to rich mixtures. In this sense, there is also a motivation in this work to analyze scenarios that are closer to those found in IC-engines operating in stratified conditions, where rich combustion can occur [51]. When focusing on the dry air scenario, the presented profiles are close. Deviations are easier to notice between the $Y_{H_2O}$ profiles, for which the MC case depicts lower values in the region where droplets penetrate into the oxidation zone (see Fig. 3). Such lower values indicate that water vapor formed by combustion reactions condensates on droplet surfaces when the MC description is enabled. The condensation is confirmed through the profiles of liquid molar fractions and the coupling source terms presented in Figs. 3 and 4. Due to the exothermic characteristic of the condensation mechanism, the temperature of both gaseous and liquid phases increases. Although minimal, this can already be noticed in the gas temperature for the dry air scenario by comparing MC and SC cases. Still, it is more pronounced in the humid air scenario. On the other hand, the increase of droplet temperature is evident in Fig. 3 for both scenarios. The heat transfer caused by the condensation mechanism, which is consequently induced by the hydrophilic nature of the fuel, partially justifies the higher flame speed values indicated in Fig. 1.

No differences in ethanol mass fraction profiles are noticed at the primary evaporation zone [52] in Fig. 2 for dry air. This is expected since droplet and gas compositions are the same in this region. However, far into the reaction zone, ethanol emerges in both cases. Differences between both profiles in dry air are justified by the slightly delayed evaporation of the remaining ethanol by

[5]In the SC approach, the droplet composition is fixed to a single species.

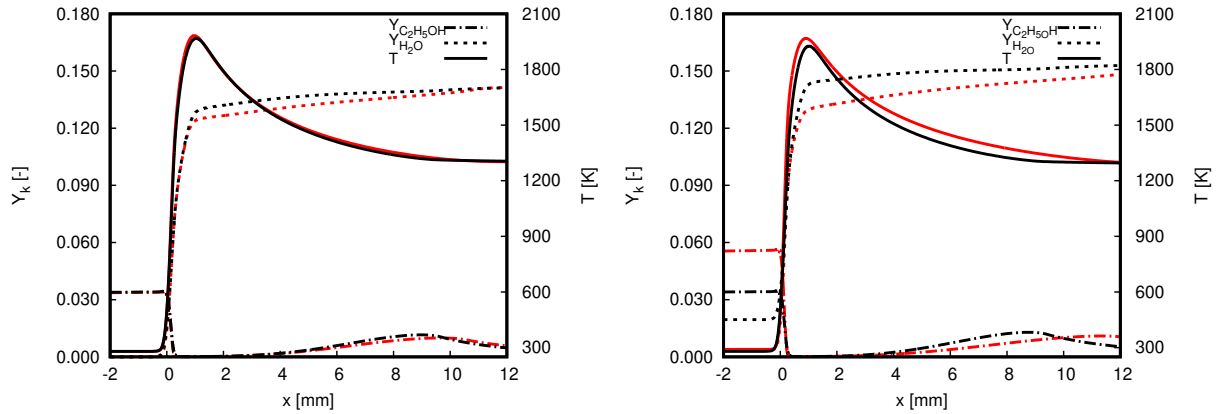


Figure 2: Evolution of the gas temperature ($T$) and the mass fractions of ethanol ($Y_{C_2H_5OH}$) and water ($Y_{H_2O}$) through the spatial coordinate $x$ at $\phi_{over} = 3.0$. On the left: dry air; on the right: humid air. SC: black; MC: red.

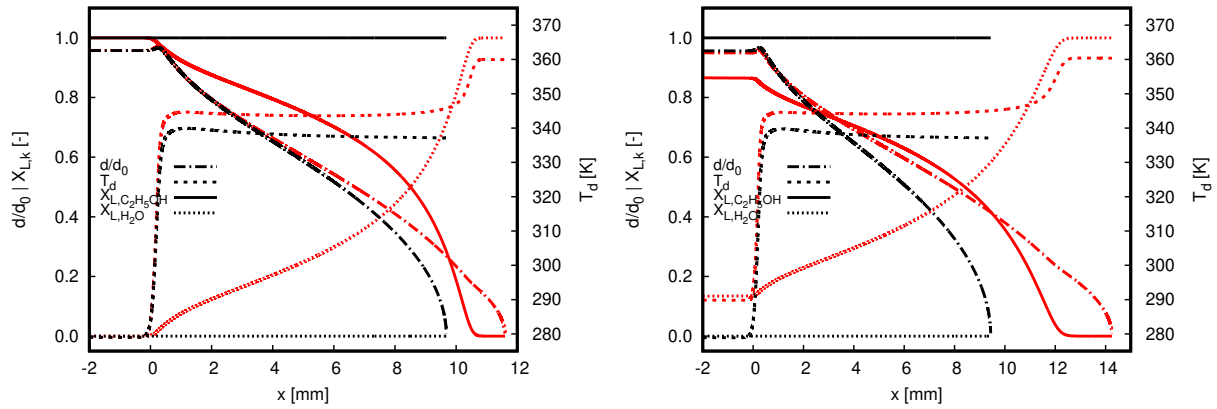


Figure 3: Evolution of the normalized droplet diameter ($d/d_0$), droplet temperature ($T_d$) and the liquid molar fractions of ethanol ($X_{L,C_2H_5OH}$) and water ($X_{L,H_2O}$) through the spatial coordinate $x$ at $\phi_{over} = 3.0$. On the left: dry air; on the right: humid air. SC: black; MC: red.

MC droplets (see $S_{C_2H_5OH}$ profile in Fig. 4), which also penetrate farther into the flame (see Fig. 3).

When comparing both scenarios, deviations in humid air are much more evident than those of dry air. Except for $Y_{C_2H_5OH}$ and $Y_{H_2O}$ profiles, the general behaviors seen for dry air are maintained for humid air. Both ethanol and water mass fraction profiles change in the primary evaporation zone between approaches because of the interaction of the hydrophilic droplets with the air humidity when enabling the MC model. Accordingly, water is allowed to condense on the droplet surface already in the primary evaporation zone, increasing the mixture temperature arriving at the flame front. It is essential to highlight that although the mixture temperature increases in the primary vaporization zone, this is a local phenomenon. Far downstream the reaction zone, burnt gases computed with both approaches reach the same temperature value as the numerical setup is adiabatic. This can already be noticed in Fig. 2. As a result, the ethanol mass fraction, as well as gas and droplet temperatures, reaching the flame are higher with the MC approach. In contrast,

the gaseous water mass fraction arriving at the reaction zone is lower with the MC approach.

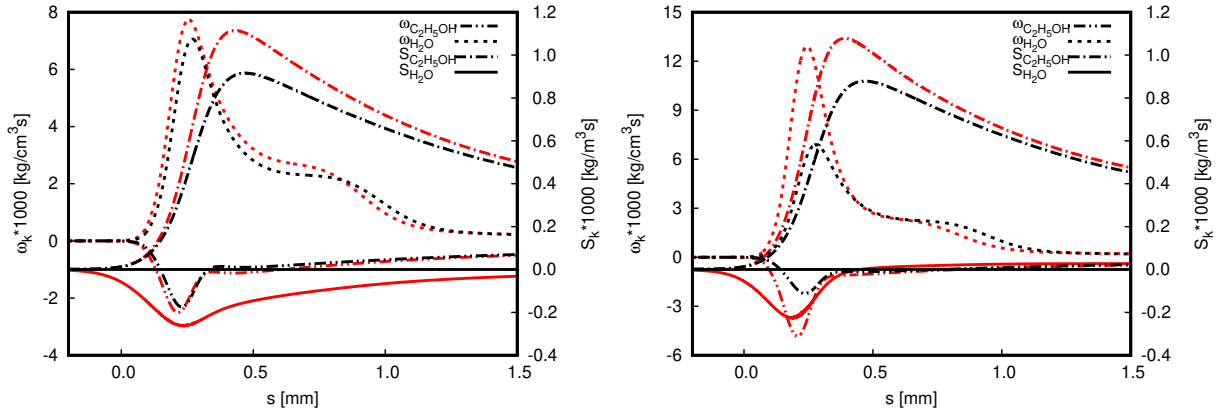


Figure 4: Evolution of reaction source terms $\dot{\omega}_k$ and coupling source terms $S_k$ for ethanol and water through the spatial coordinate $x$ at $\phi_{\text{over}} = 3.0$. On the left: dry air; on the right: humid air. SC: black; MC: red.

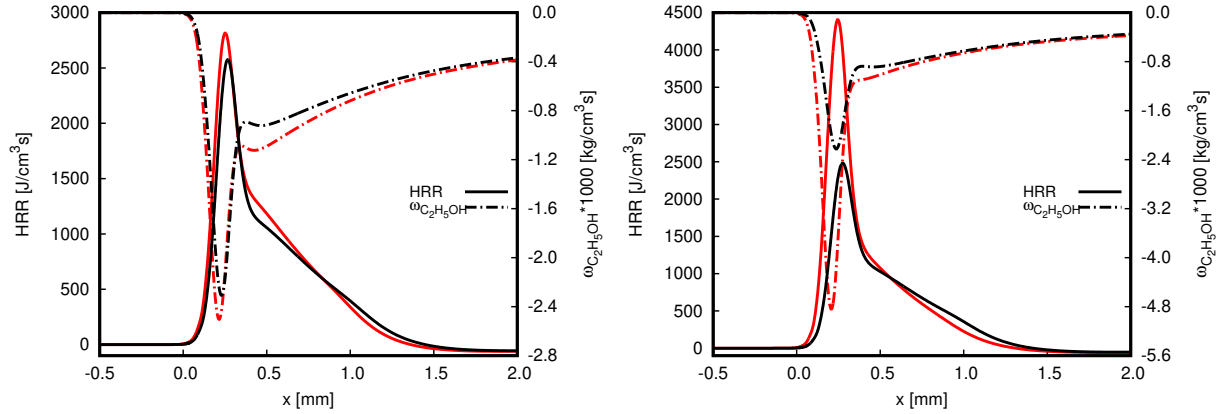


Figure 5: Evolution of the heat release rate (HRR) and the chemical source term of ethanol $\omega_{C_2H_5OH}$ through the spatial coordinate $x$ at $\phi_{\text{over}} = 3.0$. On the left: dry air; on the right: humid air. SC: black; MC: red.

Before deepening into the justification of flame speed changes, it is important to remember the procedure adopted for laminar flame speed computation. As presented in section 3, the adopted approach to compute laminar flame speeds in CHEM1D is based on quantities obtained at the inner layer, chosen as the location of the maximum heat release rate (HRR). Therefore, the main phenomena impacting flame speeds are expected to be found upstream from the region where the maximum HRR is found. As follows, the most important phenomenon observed in Fig. 4 refers to the higher values of $S_{C_2H_5OH}$ in the reaction zone for the MC case when compared with the SC approach for both dry and humid air. This shows that water condensation enhances ethanol evaporation, which can be justified by the phase equilibrium that contemplates the droplet heat-up and the change of the composition as depicted in Fig. 3. The intensification of ethanol evaporation by enabling the MC approach occurs as soon as water starts to be formed in the flame, which coincides with the reaction zone. As a consequence, fuel is directly injected into the high reaction

rates region, intensifying them and allowing for an increase in the flame propagation velocity. The proportionality between $\omega_{C_2H_5OH}$ and chemical heat release rate (HRR) profiles presented in Fig. 5 corroborates this rationale. Concerning the scenario with humid air, the HRR profile is slightly anticipated compared to its counterpart for both flames computed with the MC approach. This results from the higher mass fractions of ethanol that reach the flame front when water condensation occurs already in the primary evaporation zone.

Results achieved with the simulations conducted with the MC model and Raoult's law ($MC_R$) in Fig. 1 reinforce the discussions conducted so far and allow to go deep into the underlying physics. Concentrating on the dry air scenario, flame speed values are slightly higher than those achieved with the non-ideal VLE approach. This indicates that both VLE approaches deliver, at least, similar results in the region that impacts the flame speed calculation, which is exactly seen in Fig. 6. When comparing both VLE approaches, vapor pressures of both ethanol and water are higher for the non-ideal than the ideal approach (see Fig. 1 in [53]). Exceptions are when $X_{L,C_2H_5OH} > 0.8$ where both approaches deliver similar vapor pressure values for ethanol, and when $X_{L,C_2H_5OH} < 0.1$ where both approaches deliver similar vapor pressure values for water. Since pure ethanol is arriving at the flame and $X_{L,C_2H_5OH} > 0.8$ in the reaction zone region (i.e., $[0.0\text{mm}, 0.5\text{mm}]$), it is therefore expected that the driven mechanism for water condensation is relatively higher for the ideal approach, while the one for ethanol evaporation is the same. By comparing droplet data in Fig. 6, it is evident that water condensation is more pronounced for the $MC_R$. However, although the deviations between results presented on the left of Fig. 6 are remarkable, these are not great within and upstream from the reaction zone region. The quantities presented on the right of Fig. 6 for the $MC_R$ case show slightly higher values for $S_{C_2H_5OH}$ and $\dot{\omega}_{H_2O}$, whereas slightly smaller values for $S_{H_2O}$ and $\dot{\omega}_{C_2H_5OH}$, when compared to its non-ideal counterpart. Accordingly, the slightly higher $MC_R$ flame speed values with respect to those calculated for the MC case are originated from slightly different values of coupling and reaction source terms at the reaction zone. Differences between approaches downstream of the reaction zone do not affect flame speed calculations. Such results corroborate the previous justifications for the higher flame speed values achieved for the MC approach in comparison to those computed with the SC approach. Regarding the simulations conducted in humid air, the higher condensation of water in the primary evaporation zone for $MC_R$ case enhances the ethanol availability and increases the mixture temperature at the reaction zone, resulting in higher flame speeds when using the ideal VLE approach.

At this point, it must be kept in mind the infinite liquid conductivity and diffusivity (ILCD) simplification is used in this work. Due to the contrasting rates of diffusion transport in gaseous and liquid phases (the time scale of liquid diffusion can be one order of magnitude higher than the evaporation time scale in the present cases), a stratification of droplet composition in its interior is expected.

If it is assumed that the simulated cases are limiting conditions that deliver the highest water condensation rates when compared with cases where species stratification in the droplet interior occurs, the amount of water condensed should not be higher than 2% in mass ($X_{L,H_2O}$ is below 5% in Fig. 3) for dry air simulations at the end of the region where HRR is peaking. The deposition of this amount of water in the worst-case scenario (a stagnant shell of pure water) delivers a shell thickness of less than 0.14 $\mu$m for a droplet of 50 $\mu$m of diameter, i.e., less than 0.5% of the droplet

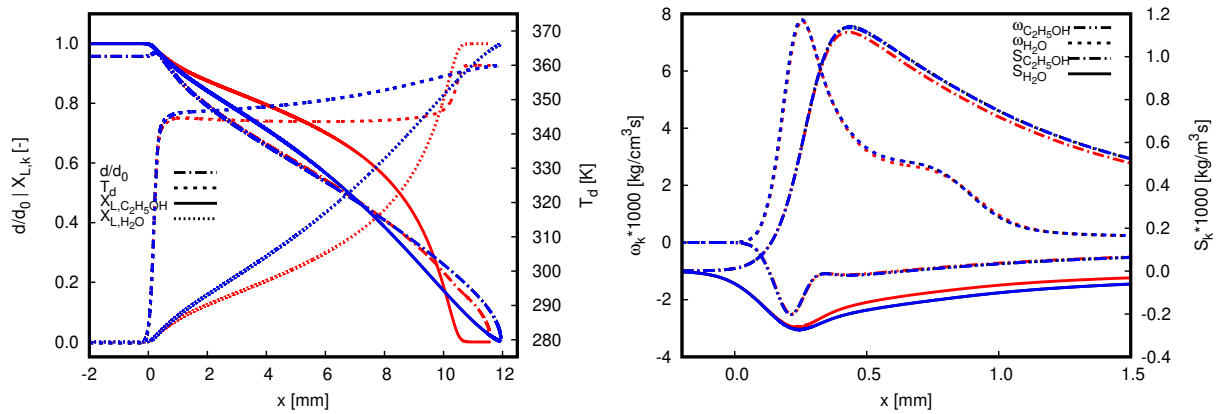


Figure 6: Evolution of selected quantities computed with the MC model and both VLE approaches in dry air through the spatial coordinate $x$ at $\phi_{\text{over}} = 3.0$. MC: red, $\text{MC}_\text{R}$: blue.

radius. In humid air simulations, which include phase change in the primary evaporation region, the film thickness should still be very low and below 2% of the droplet radius. By considering only the water condensed in the reaction zone, such a film thickness would be below 0.8% in humid air. Namely, in the worst-case scenario, the formed film is quite thin.

Nevertheless, the worst-case scenario described above is not expected to occur due to the miscibility of both species and to the mixing process in the droplet interior. As seen in Fig. 7 for the cases with pure ethanol in dry air, the slip velocity ($u_{\text{gas}} - u_d$, where $u_{\text{gas}}$ is the velocity of the gas phase and $u_d$ of the droplets) rises from zero to its maximum value exactly in the reaction zone region. As a consequence, a Hill's spherical vortex [6] is expected to be formed and, therefore, intensify the species mixing in the liquid phase. Another aspect that must be pointed out refers to the characteristics of water condensation in ethanol droplets. As seen in [54] for an ethanol droplet, the distribution of condensed water is not uniform on the droplet surface, which reinforces the low possibility of forming a homogeneous layer covering a droplet.

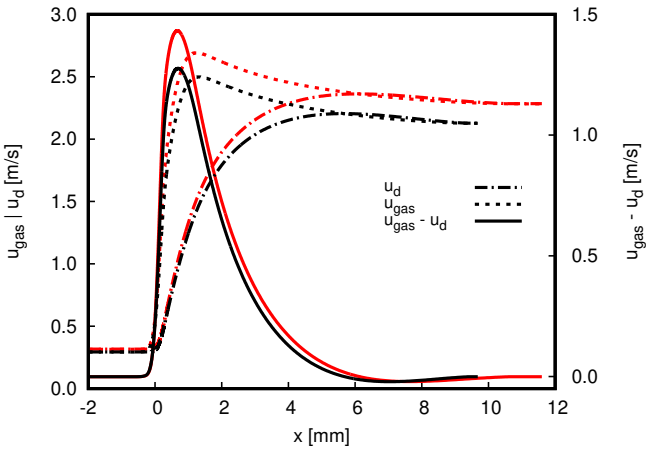


Figure 7: Velocity of the gas phase ($u_{\text{gas}}$) and droplets ($u_{\text{d}}$), as well as the slip velocity ($u_{\text{gas}} - u_d$), for flames propagating in pure ethanol droplet mists in dry air through the spatial coordinate $x$ at $\phi_{\text{over}} = 3.0$. Black: SC; red: MC approach.

Although unlikely to occur, in case a thin layer with a higher concentration of water on the droplet surface is formed , the phase change processes may not significantly contrast with those computed here. As seen in [55, 56], due to the non-ideal VLE of ethanol and water mixtures, the vapor pressure of ethanol remains high for a wide range of liquid molar fractions. Thus, forming a layer with a high water concentration involving a droplet may not significantly contrast with the achieved mass transfer rates.

From Fig. 7, it is clear that the mist is quiescent in the primary evaporation region, while in the reaction zone, the slip velocity is not low. This allows us to question the characteristics of the droplet-flow interaction. By verifying the amount of liquid in the highest $\phi_{\text{over}}$ considered in this study, it can be obtained that the spray is still in the dilute regime. Therefore, the droplet-flow interaction is expected to be negligible.

So far, analyses were concentrated on a single value of overall equivalence ratio, i.e., $\phi_{\text{over}} = 3.0$. Nevertheless, such discussions are valid throughout the computed $\phi_{\text{over}}$. To demonstrate this, Figs. 8, 9, and 10 present colormaps of selected quantities. Such colormaps were constructed with the computed flames in a grid defined by $\phi_{\text{over}}$ and the spatial coordinate $x$.

In Figs. 8 and 9 selected quantities from flames computed in both SC and MC approaches in dry air are presented and compared using deviation plots. To compute such deviations, the following expression is used $\epsilon_\psi = \psi - \psi_{\text{ref}}$, where $\psi$ refers to the compared quantity and subscripts $_{\text{ref}}$ to a reference value, i.e. the quantity specified in the caption of the colormap figures.

Gas and droplet temperatures, as well as water mass fractions in the gas phase, show similar behaviors to those previously noticed in profile plots. As the values of $\phi_{\text{over}}$ increase, droplet penetration increases and the behavior noticed for gas and droplet temperatures at $\phi_{\text{over}} = 3.0$ is replicated. However, the evolution of $Y_{H_2O}$ does not follow a regular shape throughout $\phi_{\text{over}}$. From results achieved for both SC and MC approaches, $Y_{H_2O}$ profiles depict a monotonic behavior through $x$ up to $\phi_{\text{over}} \approx 3.0$. Around this value of $\phi_{\text{over}}$, the mass fraction of water reaches a maximum. But, for mixtures richer than $\phi_{\text{over}} \approx 3.0$, the $Y_{H_2O}$ reaches a maximum between 0mm and 10mm, then slowly decreases. This occurs due to the high penetration of the droplet into the oxidation zone and the late injection of fuel and absorption of water in MC cases, as noticed through the $Y_{C_2H_5OH}$ profiles in Fig. 10 [6].

The remaining key quantities used to justify the flame speed behavior in the different scenarios are presented in Fig. 9. The coupling source terms follow the trend noticed in the profile plots. Throughout the $\phi_{\text{over}}$, no shape changes are noticed, but values are higher for cases computed with the MC approach. In contrast, the remaining source terms in Fig. 9 do not show such a regular behavior. From the leanest to the highest $\phi_{\text{over}}$, the negative peak values of $\dot{\omega}_{C_2H_5OH}$ regularly approach the position 0.0 mm and become more intense. Such a behavior is maintained until $\phi_{\text{over}} \approx 2.5$ is reached. For richer mixtures, a second one appears downstream of the first $\dot{\omega}_{C_2H_5OH}$ negative peak, indicating the decomposition of the later released ethanol by droplets into the oxidation zone. Despite this bimodal shape of $\dot{\omega}_{C_2H_5OH}$ through $x$, the HRR profiles become gradually more concentrated and intense as $\phi_{\text{over}}$ becomes higher until the corresponding value of the maximum laminar flame speed is reached. The deviation plot of HRR indicates that, as $\phi_{\text{over}}$

[6] Notice that colormaps of the MC computation in humid air are plotted in both Figs. 8 and 10.

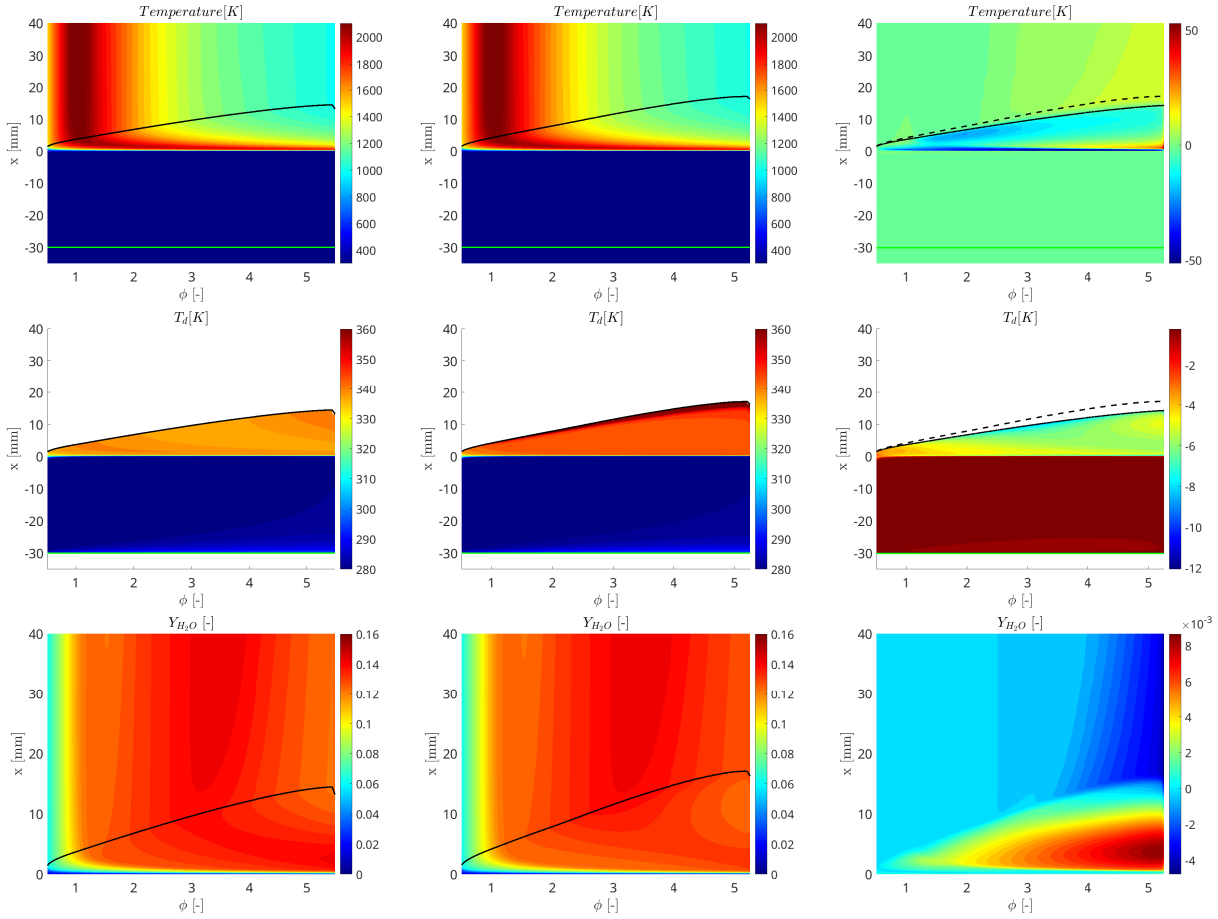


Figure 8: Colormaps of selected quantities of flames computed with the SC and the MC approaches in dry air. Left: SC; middle: MC; right: deviations between SC and MC approaches. Black line: penetration threshold for SC approach; green line: droplet injection position; dashed line: penetration threshold for MC approach in deviation plots. Reference for deviation plots: MC approach.

increases, the point where the HRR achieved with the SC approach surpasses those achieved with the MC approach (seen in Fig. 5) gradually moves upstream the flame. In both scenarios, the HRR slowly decreases for richer mixtures until the quenching point is reached. Furthermore, the deviations plots presented in Fig. 9 reinforce the alignment between $\dot{\omega}_{C_2H_5OH}$ and the HRR in the inner layer throughout $\phi_{over}$. Altogether, the colormaps presented in Figs. 8 and 9 corroborate the reasoning presented in terms of profile plots to justify the flame speed behavior noticed throughout $\phi_{over}$ in Fig. 1 when including or neglecting the MC description of hydrophilic fuels.

This section is closed by discussing the colormaps of selected quantities that are more pertinent when the MC description is enabled, in Fig. 10. The impacts of considering air humidity are clearly noticed in $Y_{C_2H_5OH}$ in Fig. 10. As with profile plots, water in the fresh reactants intensifies the primary evaporation of ethanol. This phenomenon increases with $\phi_{over}$, corroborating the justification given to the increase of the flame speed as the mixture becomes richer. Also, in $Y_{C_2H_5OH}$ colormaps, as the primary evaporation increases, less ethanol is available in the droplets and the amount of ethanol released in the oxidation zone decreases. The corresponding change in

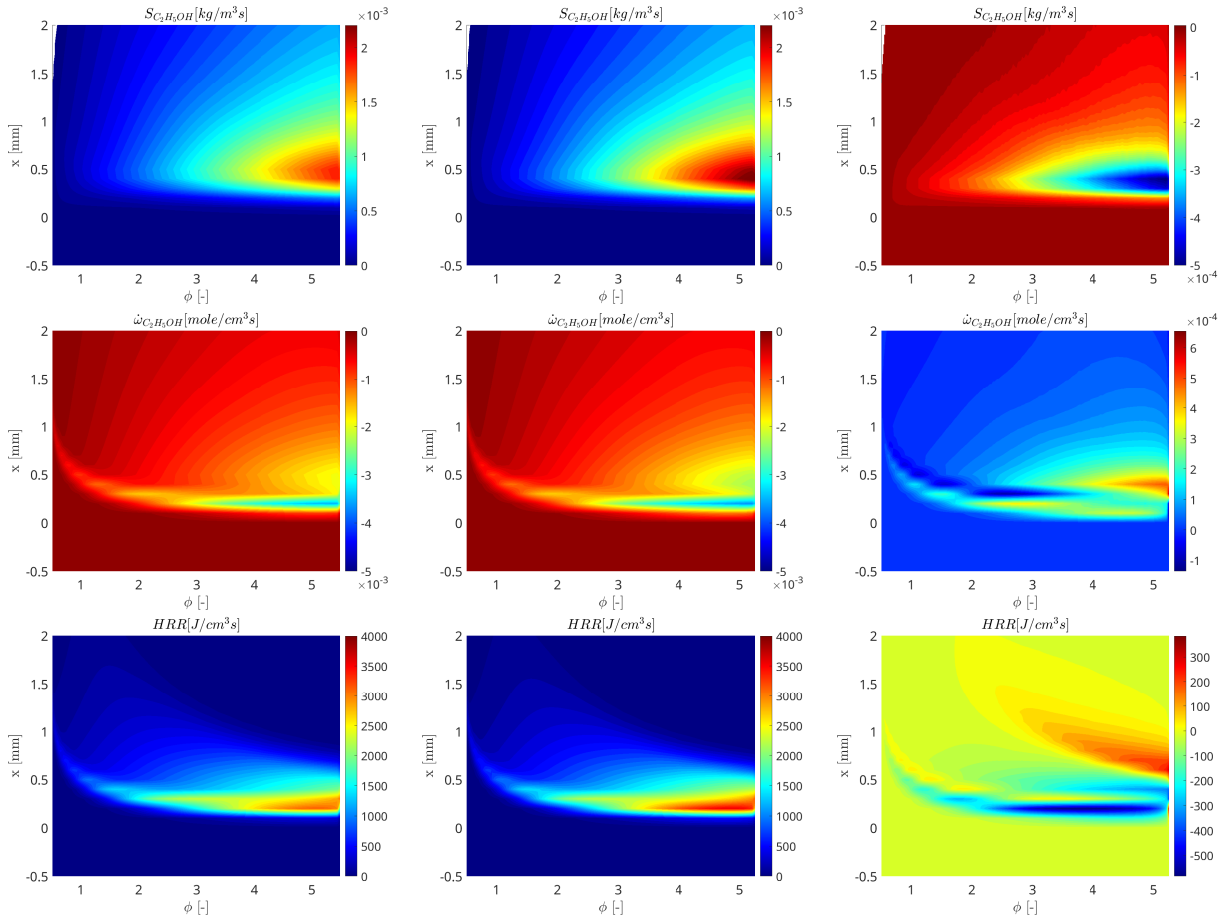


Figure 9: Colormaps of selected source terms of flames computed with the SC and the MC approaches in dry air. Left: SC; middle: MC; right: deviations between SC and MC approaches. Reference for deviation plots: MC approach.

droplet composition is reported in terms of the liquid molar fraction of fuel in the second row of Fig. 10. As a droplet moves through the flame, its composition changes from pure fuel to pure water. The presence of air humidity accelerates this process and, in this scenario, droplets interacting with flames have a higher amount of water. Further, droplets in humid air penetrate more into the oxidation zone than droplets in dry air, due to the lowers evaporation rate of water. Regarding $X_{L,\mathrm{C_2H_5OH}}$, the variation from lean to rich mixtures is obviously due to the increase in $\phi_{\mathrm{over}}$. Also, we notice that the available ethanol at the flame location is increasing with $\phi_{\mathrm{over}}$. It confirms that primary evaporation is a first source of flame speed increase, as more gaseous fuel is immediately available to feed the flame.

Another important quantity to be tracked in MC scenarios is the coupling source term of water $S_{\mathrm{H_2O}}$. By comparing humid and dry air scenarios, water starts to condense as soon as droplets are injected into a humid atmosphere. Since no water is available in the primary evaporation zone with dry air, $S_{\mathrm{H_2O}}$ is zero in this region. However, the more intense values of $S_{\mathrm{H_2O}}$ occur in the reaction zone for both cases, which are focused in Fig. 10. This is more pronounced as $\phi_{\mathrm{over}}$ increases. Further deviations are noticed in the oxidation zone due to the contrasting droplet compositions.

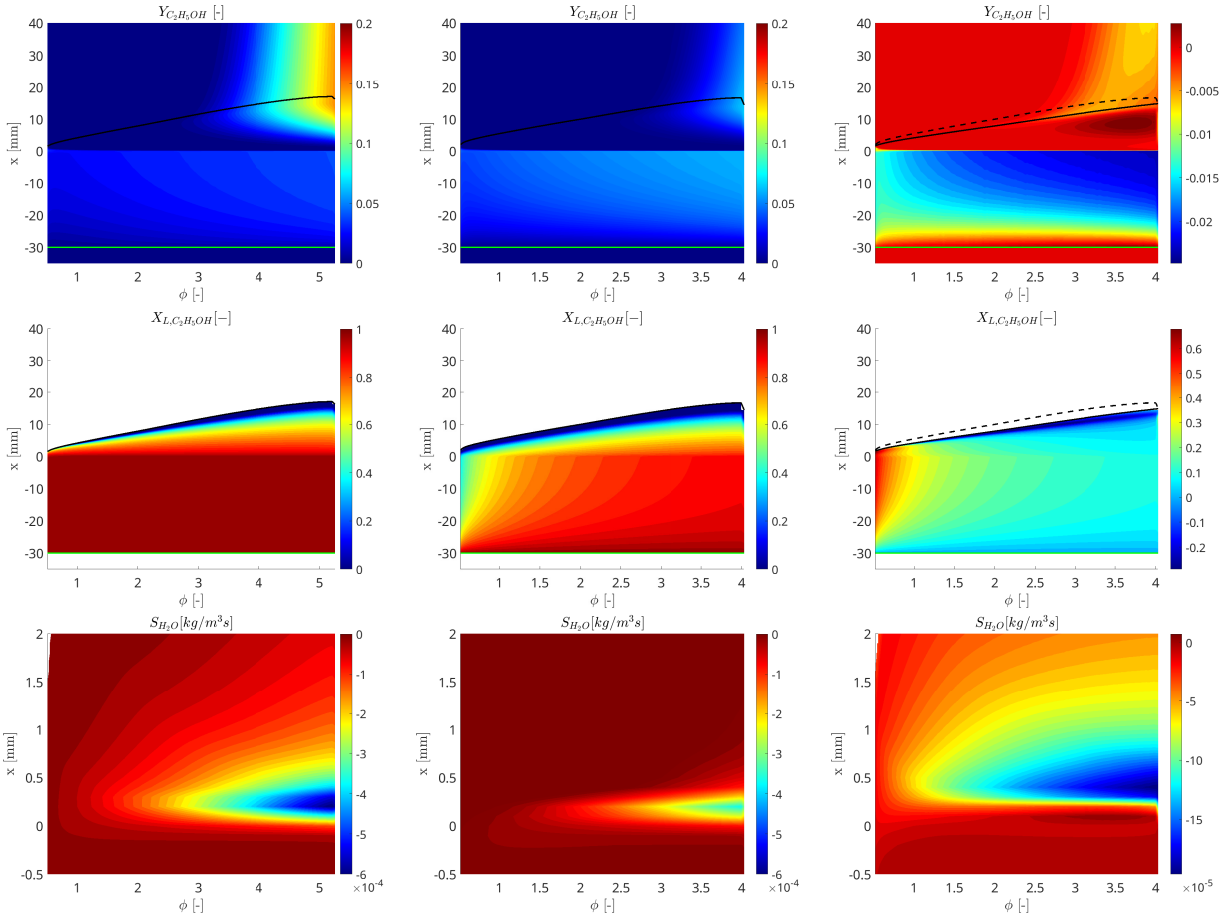


Figure 10: Colormaps of ethanol mass fraction in the gas phase ($Y_{C_2H_5OH}$), of ethanol liquid molar fraction ($X_{L,C_2H_5OH}$) and of the coupling source term of water ($S_{H_2O}$) of flames computed with the MC approach in dry and humid air. Left: dry air; middle: humid air; right: deviations between flames in dry and humid air. Black line: penetration threshold; green line: droplet injection position; dashed line: penetration threshold for humid air in deviation plots. Reference for deviation plots: humid air.

In humid air scenarios, high values of $S_{H_2O}$ in the oxidation zone indicate the low absorption of water vapor caused by the higher $X_{L,H_2O}$ values.

### *4.2. Analysis of hydrous ethanol*

Following the investigation of pure hydrophilic fuel droplets interacting with flames, it is a natural choice to analyze how such an interaction evolves for multi-component droplets composed of hydrophilic fuel and water. Throughout this section, droplets are composed of binary mixtures of ethanol and water, i.e., 92.5% of ethanol and 7.5% of water in mass, following the composition of hydrous ethanol with a higher percentage of water specified in [57].

Laminar flame speeds are presented in Fig. 11 against $\phi_{over}$, in humid and dry air. In contrast to Fig. 1, the influence of mixing water with fuel in the liquid phase follows the expected trend: the hydrous ethanol delivers lower flame speed values than the corresponding cases of pure ethanol. However, the influence of air humidity follows the same trends previously noticed for pure ethanol.

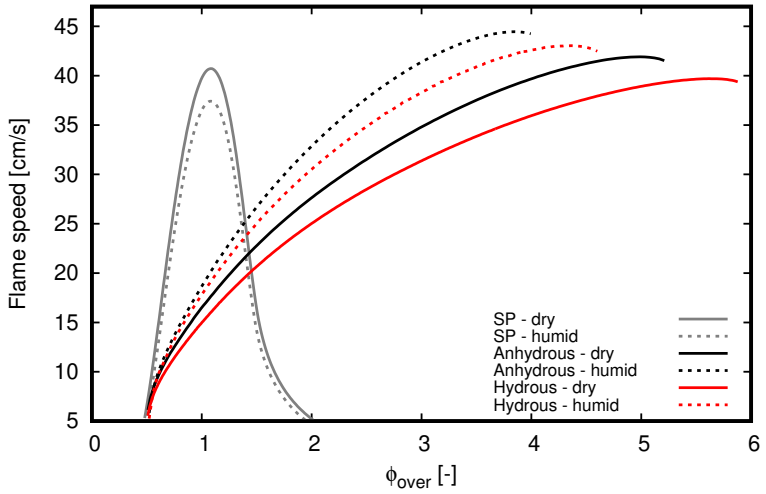


Figure 11: Laminar flame speed by equivalence ratio of single phase (SP) and two-phase freely propagating flames for humid and dry air. In all mists, the MC approach is applied.

Figures 12 and 13 present profiles plots for $\phi_{\text{over}} = 3.0$ of the same quantities as in Sec. 4.1. In view of the quantities used to justify the flame speed, differences between cases computed with hydrous ethanol in dry and humid air are more pronounced for gaseous mass fractions, liquid molar fractions, reaction rates, and HRR. The intensification of the flame speed values from dry to humid air, as seen in Fig. 11 for hydrous ethanol cases, can be justified by the higher mass fraction of ethanol arriving at the flame front. The higher release of ethanol vapor into the reaction zone does occur but is less pronounced than the primary evaporation of ethanol before reaching the flame. Accordingly, it is expected that, by reducing the droplet injection distance, flame speed values computed in dry and humid atmospheres will approach each other. However, the minimal evaporation of fuel in the primary evaporation zone and the higher release of fuel vapor straight into the reaction zone shall preserve higher flame speed values for cases computed in humid air[7].

The composition of the hydrous ethanol droplets, typical for commercial fuels in Brazil, might generate the so-called inversion problem, first documented in [3] and where the less volatile component leaves the droplet first. Simulations conducted in [3] are performed for single droplets in atmospheres with fixed or varying composition, not modified by the vapor released or collected by droplets. Within that context, it was possible to observe for binary droplets of alcohols and water that water ultimately left the droplet first. This phenomenon is suppressed by including minimal water vapor in the far-field gas. The required amount depends on the liquid composition, initial gas and liquid temperatures, and VLE and vapor pressure modeling approaches. In the present work and following the procedure applied in [3] for a fixed far field gas composition and temperature of 298K at 101.325kPa, the inversion problem is suppressed for the chosen hydrous ethanol composition for a relative humidity higher than 1.5%, i.e. $Y_{H_2O} = 0.0003$. Here, the small amount of water released by droplets in the near field of the injection allows a value of $Y_{H_2O} > 0.0003$. As

[7]With respect to the applied modeling strategy for the liquid phase, the same issues discussed for anhydrous ethanol droplets in section 4.1 do also apply for hydrous ethanol simulations.

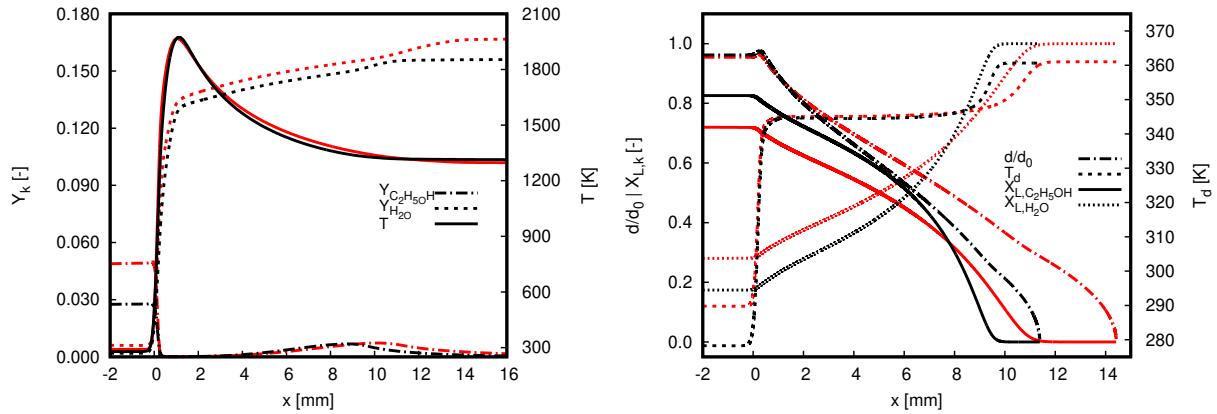


Figure 12: Evolution of carrier and dispersed phase quantities through the spatial coordinate $x$ at $\phi_{\text{over}} = 3.0$. Black: dry air; red: humid air.

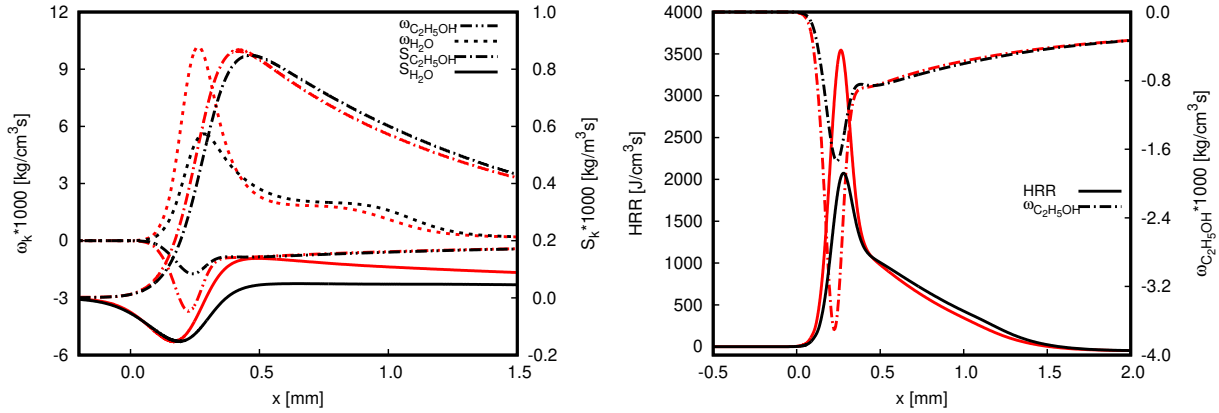


Figure 13: Evolution of selected source terms through the spatial coordinate $x$ at $\phi_{\text{over}} = 3.0$. Black: dry air; red: humid air.

a result, the inversion problem is suppressed, and the evolution of $X_{L,\mathrm{H_2O}}$ presented in Figs. 12 and 14 show that water is the last component remaining in both conditions, dry and humid air.

The results presented in Fig. 14 indicate that penetration is farther into the flame for cases computed with humid air. This behavior agrees with the previously reported results for anhydrous ethanol. The water mass fraction and liquid molar fraction colormaps point out that the interaction of droplets and the air humidity in the primary evaporation zone are the main sources of deviation between both scenarios. In humid air simulations, droplets arrive at the flames with more water. As the water evaporation rate is smaller than that of ethanol, droplets penetrate farther in the oxidation zone. The contour plots of the coupling source term $S_{\mathrm{H_2O}}$ point out the differences between both scenarios. As no humidity is present in the primary evaporation zone of the dry air simulations, this term is slightly positive for $x < 0.0$. As droplets start to interact with the flame, strong condensation occurs since $S_{\mathrm{H_2O}} < 0$. A rapid inversion to an evaporation mode ($S_{\mathrm{H_2O}} > 0$) follows as the high temperatures of the gas phase shift droplets temperature to a plateau (see Fig. 12), consequently indicating that both ethanol and water are leaving the droplets. For the colormaps of

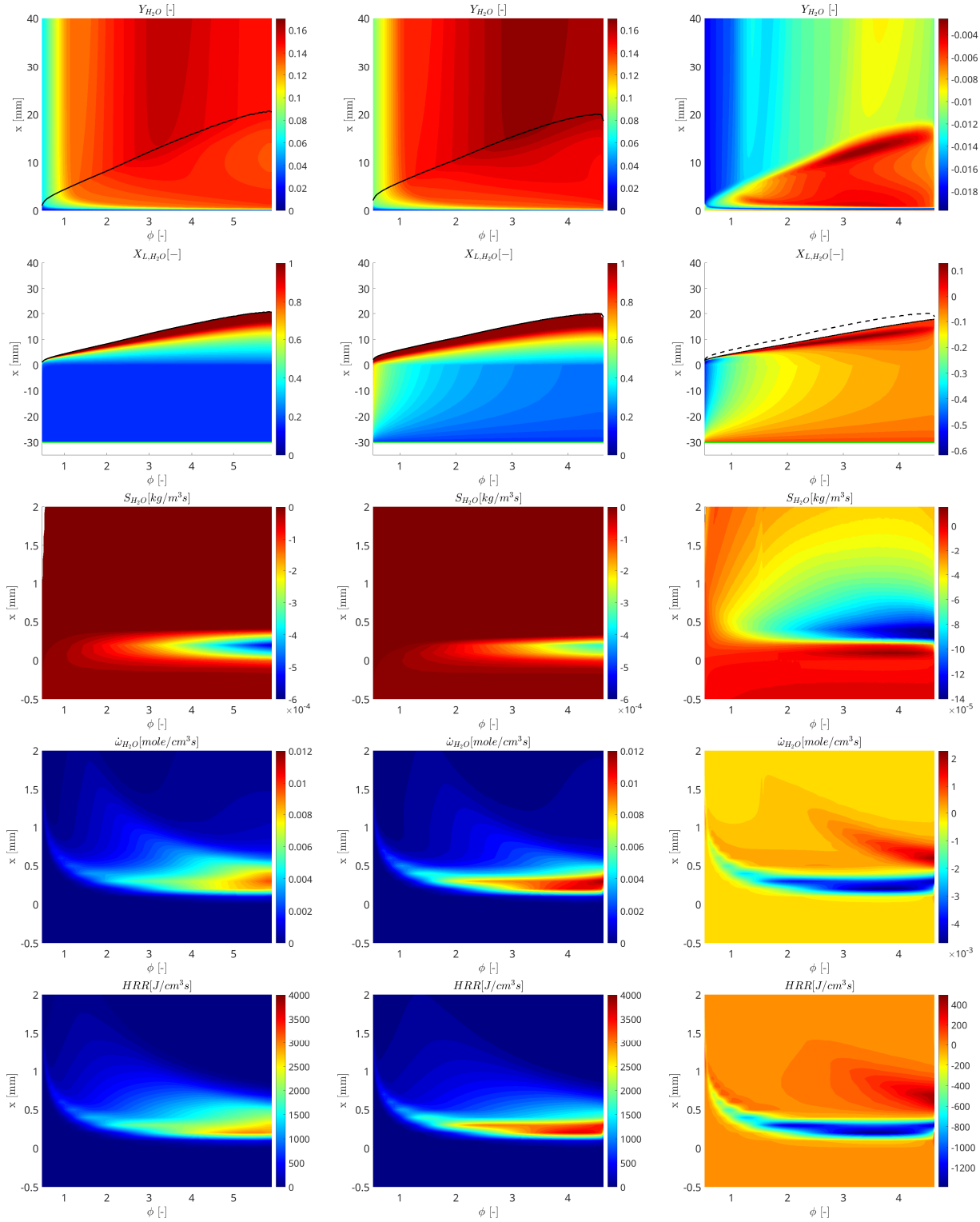


Figure 14: Colormaps of selected quantities of flames computed with hydrous ethanol in dry and humid air. Left: dry air; middle: humid air; right: deviations between flames in dry and humid air. Black line: penetration threshold; green line: droplet injection position; dashed line: penetration threshold for humid air in deviation plots. Reference for deviation plots: humid air.

$\dot{\omega}_{H_2O}$ and HRR, both depict similar behaviors. Values become more intense and concentrated with $\phi_{over}$ in a straight zone from 0.0mm to 1.0mm. Although simulations with dry air allow a larger span of $\phi_{over}$, values of both $\dot{\omega}_{H_2O}$ and HRR are predominantly more intense for the humid air case. In summary, the results presented in Fig. 14 corroborate the reasoning presented regarding profile plots to justify the higher flame speed achieved in humid rather than dry air.

### *4.3. Explanation about faster flames encountered in spray combustion*

Flames propagating in droplet mists may show higher maximum laminar flame speed values than flames in mixtures of gaseous reactants. This behavior occurs besides the higher absolute enthalpy of gaseous flames at similar overall equivalence ratios. This phenomenon was early noticed in experimental works (e.g., [58, 59]) and later reproduced numerically in one-dimensional flames described by detailed reaction mechanisms (e.g. [32, 33]). Although many rationales were used to explain such high flame speeds in the literature, none seem sufficient to justify it.

Different mathematical expressions are available to estimate the laminar flame speed ($s_l$) of gaseous flames (e.g., [60–62]). Kuehne et al. [63] present an equation that allows the computation of the consumption speed ($s_c$) in terms of the source term of a reaction progress variable $\dot{\omega}_{pv}$:

$$s_c \propto \int_{-\infty}^{\infty} \dot{\omega}_{pv} dx \; ; \quad \text{in which} \quad s_l = s_c - u_u \tag{9}$$

and $u_u$ refers to the unburnt gas velocity. Such an expression offers an advantage to analyze flames propagating in droplet mists, since according to the composition of the reaction progress variable ($Y_{pv}$), a phase coupling term can be avoided in its corresponding transport equation. As a result, a clearer connection between $s_l$ and the integral of $\dot{\omega}_{pv}$ is noticed when compared with other expressions based on the integral of the HRR and the reaction rates (e.g., summarized in [36]), which account for coupling source terms. Results presented in Fig. 15 demonstrate that the proportionality presented for gaseous flames in Eq. 9 also holds for flames propagating in droplet mists. Specifically, results presented in Fig. 15 do not coincide with the previous ones presented throughout this manuscript due to the diffusion transport model chosen for the analysis presented in this section, as explained in what follows.

During the development of the present work, some analyses have been conducted about the evolution of the spray flames in terms of the local mixture fraction ($Z$) and the reaction progress variable employed in [64], i.e. $Y_{pv} = Y_{CO_2}/M_{CO_2} + Y_{H_2O}/2.5M_{H_2O} + Y_{CO}/1.5M_{CO}$. In contrast to premixed gaseous flames, where only $Y_{pv}$ varies for a fixed $Z$, there is a simultaneous evolution of $Z$ and $Y_{pv}$ in spray flames, due to the gradual release of vapor across the flame by droplets. This was previously discussed in [33] and is plotted in Fig. 16 over a Flamelet Generated Manifold (FGM) colored by $\dot{\omega}_{pv}$. To allow a better approximation of the reaction stages among spray flames and the FGM depicted in Fig. 16, the considered spray flames in this section do not account for evaporative cooling effects (see [33]) and are based on the SC approach, with the diffusive transport being modeled following the unity Lewis number strategy by enforcing that $Sc = Pr = 0.7$. The FGM was constructed with premixed gaseous flamelets computed with the mechanism proposed in [42] for $\phi \in [0.47, 1.97]$ following a similar strategy employed in [14]. The same diffusion transport approach applied for the spray flames is used to compute the premixed gaseous flamelets. As shown in [14], simulations conducted with, virtually, the same FGM table are able to recover

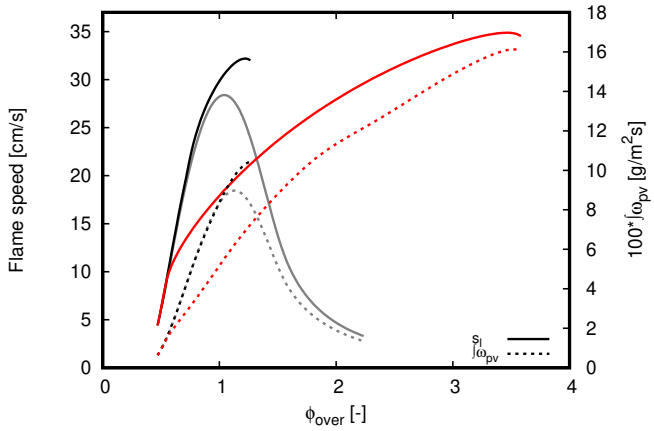


Figure 15: Laminar flame speed and $\int_{-\infty}^{\infty} \dot{\omega}_{pv} dx$ by equivalence ratio of single phase (SP) freely propagating flames and flames propagating in droplets mists with $d_d^0 = 25\mu$m and $d_d^0 = 50\mu$m. Gray: SP; black: $d_d^0 = 25\mu$m; red: $d_d^0 = 50\mu$m.

the laminar flame speed of flames propagating in droplets mists for a range of $\phi_{\text{over}}$ and $d_d^0$. In Fig. 16 the paths of the fastest flames found in Fig. 15 for the gaseous flames and for those associated with the $d^0 = 25\ \mu$m and $d^0 = 50\ \mu$m mists are traced over a $\dot{\omega}_{pv}$ manifold.

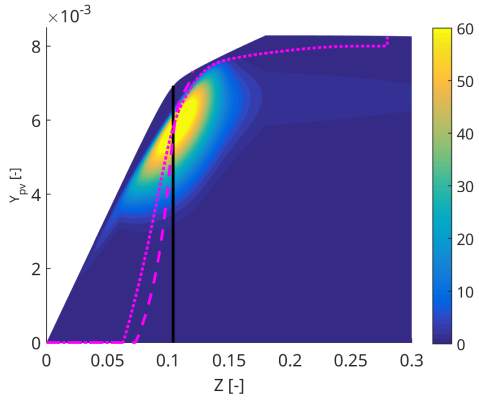


Figure 16: Flame paths ploted over a Flamelet Generated Manifold colored by $\dot{\omega}_{pv}$. Black line refers to the fastest gaseous flame while magenta refers to flames propagating in droplet mists. Dashed line: $d_d^0 = 25\mu$m and dotted line: $d_d^0 = 50\mu$m.

By analyzing the evolution of flames propagating in droplet mists in Fig. 16 it turns out that, according to the vapor release rate across the flame, reaction paths are able to cross a broader region of high values of $\dot{\omega}_{pv}$ when compared to premixed gaseous flames. Figure 17 presents profiles of $\dot{\omega}_{pv}$ and of HRR for the three flames traced over the FGM in Fig. 16. As noticed, the flames propagating in droplets mists depict broader regions where $\dot{\omega}_{pv} > 0$.

In conclusion, the distribution of fuel throughout the flame by the mass transfer among phases leads to an increase in the reaction rate, which consequently impacts the flame speed. On one hand, in terms of a valid progress variable, the fuel injection into the carrier phase by the coupling source

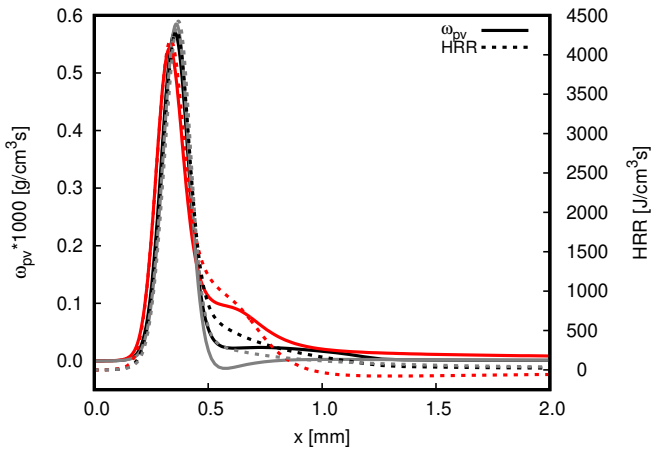


Figure 17: Development of $\dot{\omega}_{pv}$ and HRR throughout the spacial coordinate $x$ for the three flames traced over the FGM in Fig. 16. Gray: SP; black: $d_d^0 = 25\mu$m; red: $d_d^0 = 50\mu$m.

terms allows further formation of combustion products at high reaction rates, which is revealed by the continuous and distributed values of $\dot{\omega}_{pv}$ throughout the flame. On the other hand, the interaction between droplets and flames adds fuel enthalpy throughout the reaction zone, allowing the enhancement of the heat release rate within the reaction zone. As a result, flame speed is intensified when compared to gaseous combustion. This observation is not restricted to flames neglecting the evaporative cooling and is not specific to the unity Lewis number approach.

## 5. Conclusions

Flames propagating in droplet mists were simulated with a detailed description of the chemistry and the diffusion transport for different hydrophilic fuel compositions to pose the importance of considering the multi-component description of liquid fuels. Analyses systematically evolve from single to two-phase flows and single to multi-component modeling approaches. To rigorously account for the differential diffusion of vapor into the gas flow, the approach proposed in [14] was applied. New findings are presented regarding the flame speed, which were carefully justified throughout the manuscript. In addition, a new justification is presented for the observed higher flame speed values of flames propagating in droplet mists when compared to single-phase flames. The results show that describing a hydrophilic fuel as a single-component substance suppresses the description of essential phenomena for reacting two-phase flows.

Results are first concentrated on simulations of flames propagating in sprays of a pure hydrophilic fuel. Therein, important findings were obtained. As soon as the multi-component approach is enabled, flame speeds become higher than those achieved with the single-component approach. Very contrasting is the inverse behavior of the flame speed values when computations were performed considering humid air. Instead of being reduced, as seen for single phase flames or for flames in mists using the single component approach, flames in humid air propagate faster by including multi-component phenomena. These phenomena could be properly justified by the detailed description of each species' heat and mass transfer mechanisms, as allowed by the adopted modeling strategy.

Then, investigations of flames propagating in droplet mists formed by binary mixtures of ethanol and water were conducted. In general, behaviors noticed for pure ethanol droplets are reproduced for hydrous ethanol. Nevertheless, hydrous ethanol flame speeds are lower than those obtained with pure ethanol droplets given a specific atmosphere. Special attention is paid to the so-called inversion problem, noticed in [3]. However, the two-way coupling, included for the first time with the approach proposed in [14], inhibits such a phenomenon for the simulated setups as water vapor becomes present in the far field.

Specifically from the investigations conducted with a pure fuel in dry air, it turns out that the multi-component description of the droplet heat and mass transfer is necessary to properly describe the impact of the fuel's hydrophilicity on flame propagation. Without properly accounting for the vapor transport in droplet heat and mass transfer models, important phenomena for reacting spray flows are suppressed.

The investigations accounting for air humidity indicate that this quantity influences basic flame characteristics. Although the extent of such an influence may depend on the adopted modeling strategies (such as the description of the droplet interior and the consideration of spherical symmetry), it's existence became evident through the conducted analyses. We highlight that the achieved results have not been observed experimentally so far, as it is not a common practice to control air humidity in reacting flow measurements. Therefore, the achieved outcomes can also be used as a motivation for subsequent experimental analyses. Further investigations considering a more detailed descriptions of the droplet interior are desired, and these are left for future works.

The present study is also expected to contribute to the technological development for the usage of biofuels. A particular focus was given to ethanol due to its increasing usage for transportation purposes. However, other alcohols, such as methanol and ketones, are expected to demonstrate the same behavior because of their corresponding hydrophilic characteristic.

## Acknowledgements

We acknowledge the financial support from São Paulo Research Foundation (FAPESP - grant # 2021/14245-1). The support of the Human Resources Program (PRH) of the Brazilian National Agency for Petroleum, Natural Gas and Biofuels (ANP), of Fundação de Desenvolvimento da Pesquisa - Fundep, Rota 2030 - Linha V and of Coordenação de Aperfeiçoamento de Pessoal de Nível Superior – Brasil (CAPES) – Finance Code 001 are also acknowledged.

## References

[1] V. Shastry, Q. Cazeres, B. Rochette, E. Riber, B. Cuenot, Numerical study of multicomponent spray flame propagation, Proc. Combust. Inst. 38 (2021) 3201–3211.

[2] M. Bonanni, M. Ihme, Interaction of preferential evaporation and low-temperature chemistry in multicomponent counterflow spray flames, Proc. Combust. Inst. (2022).

[3] F. L. S. Filho, A. C. Santos, A. Vié, G. C. K. Filho, A new robust modeling strategy for multi-component droplet heat and mass transfer in general ambient conditions, Int. J. Heat Mass Transfer 194 (2022) 123102.

[4] A. C. Santos, F. L. S. Filho, A. Vié, The general formulation of the energy equation and the impact of enthalpy diffusion on multi-component droplet heat and mass transfer, Int. J. Heat Mass Transfer 210 (2023) 124172.

[5] S. S. Sazhin, Advanced models of fuel droplet heating and evaporation, Prog. Energy Comb. Sci. 32 (2006) 162–214.

[6] W. A. Sirignano, Fluid Dynamics and transport of droplets and sprays, 2nd ed., Cambridge University Press, 2010.
[7] V. Ebrahimian, C. Habchi, Towards a predictive evaporation model for multi-component hydrocarbon droplets at all pressure conditions, Int. J. Heat Mass Transfer 54 (2011) 3552–3565.
[8] L. Zhang, S. C. Kong, Multicomponent vaporization modeling of bio-oil and its mixtures with other fuels, Fuel 95 (2012) 471–480.
[9] S. Tonini, G. E. Cossali, An exact solution of the mass transport equations for spheroidal evaporating drops, Int. J. Heat Mass Transfer 60 (2013) 236–240.
[10] G. Lupo, C. Duwig, A numerical study of ethanol-water droplet evaporation, J. Eng. Gas Turbines Power 140 (2018) 21401.
[11] A. P. Pinheiro, O. Rybdylova, I. A. Zubrilin, S. S. Sazhin, F. L. S. Filho, J. M. Vedovotto, Modelling of aviation kerosene droplet heating and evaporation using complete fuel composition and surrogates, Fuel 305 (2021).
[12] P. Keller, A. Bader, C. Hasse, The influence of intra-droplet heat and mass transfer limitations in evaporation of binary hydrocarbon mixtures, Int. J. Heat Mass Transfer 67 (2013) 1191–1207.
[13] B. Franzelli, A. Vié, M. Boileau, B. Fiorina, N. Darabiha, Large eddy simulation of swirled spray flame using detailed and tabulated chemical descriptions, Flow Turb. Combust. 98 (2017) 633–661.
[14] F. L. S. Filho, A. Hosseinzadeh, A. Sadiki, J. Janicka, On the interaction between turbulence and ethanol spray combustion using a dynamic wrinkling model coupled with tabulated chemistry, Combust. Flame 215 (2020) 203–220.
[15] H. Miyagawa, M. Nagaoka, K. Ohsawa, T. Yamada, Spray vaporization model for multi-component gasoline, JSAE Review 19 (1998) 299–304.
[16] L. F. T. Leite, P. L. C. Lage, Modeling of emulsion droplet vaporization and combustion including microexplosion analysis, Combust. Sci. Tech. 157 (2000) 213–242.
[17] C. Wang, A. M. Dean, H. Zhu, R. J. Kee, The effects of multicomponent fuel droplet evaporation on the kinetics of strained opposed-flow diffusion flames, Combust. Flame 160 (2013) 265–275.
[18] T. Kitano, J. Nishio, R. Kurose, S. Komori, Evaporation and combustion of multicomponent fuel droplets, Fuel 136 (2014) 219–225.
[19] P. B. Govindaraju, M. Ihme, Group contribution method for multicomponent evaporation with application to transportation fuels, Int. J. Heat Mass Transfer 102 (2016) 833–845.
[20] A. Stagni, L. Esclapez, P. Govindaraju, A. Cuoci, T. Faravelli, M. Ihme, The role of preferential evaporation on the ignition of multicomponent fuels in a homogeneous spray/air mixture, Proc. Combust. Inst. 36 (2017) 2483–2491.
[21] P. B. Govindaraju, T. Jaravel, M. Ihme, Coupling of turbulence on the ignition of multicomponent sprays, Proc. Combust. Inst. 37 (2019) 3295–3302.
[22] C. K. Law, T. Y. Xiong, C. Wang, Alcohol droplet vaporization in humid air, Int. J. Heat Mass Transfer 30 (1987) 1435–1443.
[23] A. Millán-Merino, E. Fernández-Tarrazo, M. Sánchez-Sanz, Theoretical and numerical analysis of the evaporation of mono- and multicomponent single fuel droplets, J. Fluid Mech. 910 (2021).
[24] A. C. Santos, F. L. S. Filho, A. Vié, A reference formulation for computing mass transfer rates of multicomponent droplets undergoing general phase-change, International Journal of Heat and Mass Transfer 222 (2024) 125185.
[25] P. Versaevel, Combustion laminaire diphasique etude théorique et expérimentale (1996) 1–244.
[26] G. Castanet, F. Lemoine, Heat transfer within combusting droplets, Proc. Combust. Inst. 31 II (2007) 2141–2148.
[27] A. Vié, B. Franzelli, Y. Gao, T. Lu, H. Wang, M. Ihme, Analysis of segregation and bifurcation in turbulent spray flames: A 3d counterflow configuration, Proc. Combust. Inst. 35 (2015) 1675–1683.
[28] P. M. Oliveira, Ignition and propagation mechanisms of spray flames (2019).
[29] G. Parant, L. Zimmer, A. Renaud, . Richecoeur, Adaptation of a ptv method for droplets evaporating in vicinity of a flame, Exp. Fluids 63 (2022) 100.
[30] D. Fredrich, A. Giusti, Numerical investigation of multi-component droplet evaporation and autoignition for aero-engine applications, Combustion and Flame 241 (2022) 112023.

[31] J. Wang, P. M. de Oliveira, R. S. Pathania, I. E. Helou, E. Mastorakos, Stability and structure of lean swirling spray flames with various degrees of prevaporization, Int. J. Spray Combust. Dyn. 15 (2023) 91–104.
[32] A. Neophytou, E. Mastorakos, Simulations of laminar flame propagation in droplet mists, Combust. Flame 156 (2009) 1627–1640.
[33] F. L. S. Filho, N. Speelman, J. A. van Oijen, L. P. H. de Goey, A. Sadiki, J. Janicka, Numerical analyses of laminar flames propagating in droplet mists using detailed and tabulated chemistry, Combust. Theory Model. 22 (2018) 998–1032.
[34] F. L. S. Filho, G. C. K. Filho, J. A. van Oijen, A. Sadiki, J. Janicka, A novel strategy to accurately represent the carrier gas properties of droplets evaporating in a combustion environment, Int. J. Heat Mass Transfer 137 (2019) 1141–1153.
[35] B. Rochette, E. Riber, B. Cuenot, Effect of non-zero relative velocity on the flame speed of two-phase laminar flames, Proc. Combust. Inst. 37 (2019) 3393–3400.
[36] F. L. S. Filho, L. E. de Albuquerque Paixão e Freire de Carvalho, J. A. van Oijen, G. C. K. Filho, Effects of reaction mechanisms and differential diffusion in oxy-fuel combustion including liquid water dilution, Fluids 6 (2021) 47.
[37] B. Somers, The simulation of flat flames with detailed and reduced chemical models, Ph. D. Dissertation. (1994) 195.
[38] J. A. van Oijen, L. P. H. de Goey, Modelling of premixed counterflow flames using the flamelet-generated manifold method, Combust. Theory Model. 6 (2002) 463–478.
[39] J. A. van Oijen, A. Donini, R. J. M. Bastiaans, J. H. M. ten Thije Boonkkamp, L. P. H. de Goey, State-of-the-art in premixed combustion modeling using flamelet generated manifolds, Prog. Energy Comb. Sci. 57 (2016) 30–74.
[40] A. Ern, V. Giovangigli, Fast and accurate multicomponent transport property evaluation, J. Comput. Phys. 120 (1995) 105–116.
[41] N. Leplat, P. Dagaut, C. Togbé, J. Vandooren, Numerical and experimental study of ethanol combustion and oxidation in laminar premixed flames and in jet-stirred reactor, Combustion and Flame 158 (2011) 705–725.
[42] N. M. Marinov, A detailed chemical kinetic model for high temperature ethanol oxidation, Int. J. Chem. Kinet. 31 (1999) 183–220.
[43] B. Abramzon, W. A. Sirignano, Droplet vaporization model for spray combustion calculations, Int. J. Heat Mass Transfer 32 (1989) 1605–1618.
[44] D. F. Fairbanks, C. R. Wilke, Diffusion coefficients in multicomponent gas mixtures, Ind. Eng. Chem. 42 (1950) 471–475.
[45] E. N. Fuller, K. Ensley, J. C. Giddings, Diffusion of halogenated hydrocarbons in helium. the effect of structure on collision cross sections, J. Phys. Chem. 73 (1969) 3679–3685.
[46] B. E. Poling, J. M. Prausnitz, J. P. O'Connell, The Properties of Gases and Liquids, 5th ed., McGRAW-HILL, 2001.
[47] L. P. H. de Goey, J. H. M. ten Thije Boonkkamp, A flamelet description of premixed laminar flames and the relation with flame stretch, Combustion and Flame 119 (1999) 253–271.
[48] F. L. S. Filho, Novel approach toward the consistent simulation of turbulent spray flames using tabulated chemistry (2017) 254.
[49] J. R. Cash, A. H. Karp, A variable order runge-kutta method for initial value problems with rapidly varying right-hand sides, ACM Transactions on Mathematical Software (TOMS) 16 (1990) 201–222.
[50] J. Liang, G. Li, Z. Zhang, Z. Xiong, F. Dong, R. Yang, Experimental and numerical studies on laminar premixed flames of ethanol–water–air mixtures, Energy Fuels 28 (2014) 4754–4761.
[51] G. C. K. Filho, F. M. F. Silva, A. L. Pacífico, F. L. S. Filho, C. B. Zabeu, F. B. Nigro, O. M. França, A. Penaranda, P. T. Lacava, Extended coherent flame model applied to an optical single-cylinder engine fueled with ethanol, Appl. Therm. Eng. 236 (2024) 121399.
[52] I. Silverman, J. B. Greenberg, Y. Tambour, Stoichiometry and polydisperse effects in premixed spray flames, Combust. Flame 93 (1993) 97–118.
[53] V. Y. Borodulin, M. I. Nizovtsev, A. N. Sterlyagov, Evaporation of non-ideal binary solution drops, J. Phys.: Conf. Ser. 1382 (2019) 012106.

[54] A. N. Sterlyagov, M. I. Nizovtsev, V. N. Letushko, Experimental study of evaporation of droplets of water ethanol solution at high relative air humidity, J. Phys.: Conf. Ser. 2057 (2021) 012059.
[55] K. D. O'Hare, P. L. Spedding, Evaporation of a binary liquid mixture, The Chemical Engineering Journal 48 (1992) 1–9.
[56] V. Y. Borodulin, V. N. Letushko, M. I. Nizovtsev, A. N. Sterlyagov, Influence of relative air humidity on evaporation of water–ethanol solution droplets, Colloid Journal 83 (2021) 277–283.
[57] ANP, Resolução anp nº 907, de 18 de novembro de 2022 - dou de 23-11-2022, 2022.
[58] S. Hayashi, S. Kumagai, T. Sakai, Propagation velocity and structure of flames in droplet-vapor-air mixtures, Combust. Sci. Tech. 15 (1977) 169–177.
[59] H. Nomura, K. Izawa, Y. Ujiie, J. Sato, Y. Marutani, M. Kono, H. Kawasaki, An experimental study on flame propagation in lean fuel droplet-vapor-air mixtures by using microgravity conditions, Symp. Combust. Proc. 27 (1998) 2667–2674.
[60] F. A. Williams, Combustion Theory, (1985), 2 ed., Addison Wesley, 1985.
[61] K. K. Kuo, Principles of combustion, 2 ed., John Wiley and Sons Inc., 2005.
[62] T. Poinsot, D. Veynante, Theoretical and numerical Combustion, 2 ed., 2005.
[63] J. Kuehne, A. Ketelheun, J. Janicka, Analysis of sub-grid pdf of a progress variable approach using a hybrid les/tpdf method, Proc. Combust. Inst. 33 (2011) 1411–1418.
[64] F. L. S. Filho, L. Dressler, A. Hosseinzadeh, A. Sadiki, G. C. K. Filho, Investigations of evaporative cooling and turbulence flame interaction modeling in ethanol turbulent spray combustion using tabulated chemistry, Fluids 4 (2019) 187.